INTERNATIONAL JOURNAL FOR NUMERICAL METHODS IN FLUIDS, VOL. 13, 309–319 (1991)

# TRANSONIC VISCOUS–INVISCID INTERACTION BY A FINITE ELEMENT METHOD

M. M. HAFEZ*
*University of California, Davis, CA, U.S.A.*

W. G. HABASHI*
*Concordia University, Montreal, Quebec, Canada*

AND

S. M. PRZYBYTKOWSKI
*Pratt & Whitney Canada Inc., Longueuil, Quebec, Canada*

## SUMMARY

A method is outlined for solving two-dimensional transonic viscous flow problems, in which the velocity vector is split into the gradient of a potential and a rotational component. The approach takes advantage of the fact that for high-Reynolds-number flows the viscous terms of the Navier–Stokes equations are important only in a thin shear layer and therefore solution of the full equations may not be needed everywhere. Most of the flow can be considered inviscid and, neglecting the entropy and vorticity effects, a potential model is a good approximation in the flow core. The rotational part of the flow can then be calculated by solution of the potential, streamfunction and vorticity transport equations. Implementation of the no-slip and no-penetration boundary conditions at the walls provides a simple mechanism for the interaction between the viscous and inviscid solutions and no extra coupling procedures are needed. Results are presented for turbulent transonic internal choked flows.

KEY WORDS Viscous–inviscid interaction Shock wave–boundary layer interaction Boundary layers Finite element method for flow problems Zonal methods Choked viscous flows Stream function–vorticity formulation

## INTRODUCTION

The problem of numerical simulation of viscous compressible flows is a difficult one. For two-dimensional flows over aerofoils a boundary layer is developed adjacent to the solid surface and interacts with the shock waves. The standard methods for the calculation of such phenomena are based on the time-dependent form of the Navier–Stokes equations using explicit finite difference methods based on the MacCormack scheme[1] or implicit ones based on the Beam and Warming algorithm.[2] An alternative approach based on viscous–inviscid interaction procedures has been proposed by many authors.[3–8] These methods can be essentially classified in three categories: direct, inverse and semi-inverse or quasi-simultaneous. While the classical direct method of solving boundary layers with a prescribed pressure gradient is well known to be limited to weak

* Consultant, Pratt & Whitney Canada Inc.

0271–2091/91/130309–11$05.50

*Received February 1990*

interaction problems, solving the boundary layer equations in the inverse mode may not be recommended for separated transonic flows. The semi-inverse method and the simultaneous iterative methods have been developed to avoid the difficulties of the above two approaches and have been tested with reasonable success. Unfortunately, these methods are not necessarily very efficient for general problems.

In the present work a new approach is presented that takes advantage of the fact that for high-Reynolds-number flows most of the flow can be considered inviscid and, neglecting the entropy and vorticity effects, a potential model is a good approximation in the flow core. In the viscous region it is proposed to combine potential calculations with the stream function–vorticity formulation to produce an approximate Navier–Stokes solver.

Unlike viscous–inviscid interaction methods, no explicit coupling procedure is needed in the present approach. The difficulties, in separated flow cases, associated with solving direct boundary layer equations with specified pressure gradients are hence avoided. Moreover, the present method allows for a pressure variation across the viscous layer.

In the following sections, details of the method are discussed and its numerical implementation by a finite element technique is demonstrated.

## PROBLEM DESCRIPTION AND GOVERNING EQUATIONS

According to the Helmholtz theorem, any velocity vector can be decomposed into the gradient of a scalar and a rotational component:

$$\mathbf{q} = \nabla\Phi + \nabla \times \mathbf{A}/\rho. \tag{1}$$

The first term is curl-free, while the second is divergence-free. For 2D problems the following decomposition could be used without loss of generality:

$$u = \Phi_x + \psi_y/\rho, \qquad v = \Phi_y - \psi_x/\rho, \tag{2}$$

where $\psi$ is a perturbation stream function allowing for rotational effects.

The continuity equation becomes

$$(\rho\Phi_x)_x + (\rho\Phi_y)_y = 0. \tag{3}$$

The perturbation stream function–vorticity ($\psi$–$\omega$) system is governed by the following equations:

$$(\psi_x/\rho)_x + (\psi_y/\rho)_y = -\omega, \tag{4}$$

$$\nabla^2(\mu\omega) - Re[(\rho\Phi_x + \psi_y)\omega_x + (\rho\Phi_y - \psi_x)\omega_y + S_\rho] + 2S_\mu = 0, \tag{5}$$

where

$$S_\rho = \rho_x(q^2)_y/2 - \rho_y(q^2)_x/2,$$

$$S_\mu = \mu_x(u_{xy} + v_{yy}) - \mu_y(u_{xx} + v_{xy}) - \mu_{xy}(u_x - v_y) + \mu_{xx}u_y - \mu_{yy}v_x.$$

In the present work the term $S_\mu$ is considered small and is neglected.

The formulation is completed with the following boundary conditions (Figure 1). At the inlet, $u$ is a prescribed profile; hence

$$\Phi_n = \text{given}, \tag{6a}$$

$$\psi = \text{given}, \tag{6b}$$

$$\omega = \text{given}. \tag{6c}$$

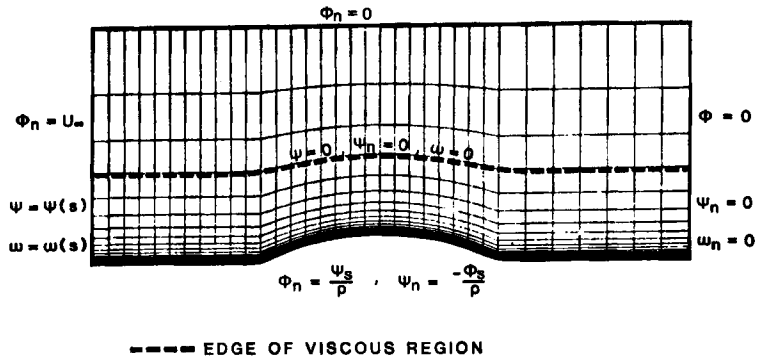


Figure 1. Proposed viscous–inviscid approach ($\Phi$–$\psi$–$\omega$) and its boundary conditions

At the exit, the streamlines are parallel:

$$\Phi = 0, \tag{7a}$$

$$\psi_n = 0, \tag{7b}$$

$$\omega_n = 0. \tag{7c}$$

At a solid stationary or moving surface,

$$v = 0, \tag{8a}$$

$$u = 0. \tag{8b}$$

In terms of $\Phi$ and $\psi$, equations (8a) and (8b) are imposed as follows:

$$\rho\Phi_n = \psi_s, \tag{9a}$$

$$\psi_n/\rho = -\Phi_s. \tag{9b}$$

At the edge of the viscous layer,

$$\psi = 0, \tag{10a}$$

$$\psi_n = 0, \tag{10b}$$

$$\omega = 0. \tag{10c}$$

*Weak-Galerkin formulation*

A weighted residual finite element procedure is used to discretize the equations. The weighted residual forms of the equations are

$$\iint W_1[(\rho\Phi_x)_x + (\rho\Phi_y)_y]\,\mathrm{d}A = 0, \tag{11a}$$

$$\iint W_2[(\psi_x/\rho)_x + (\psi_y/\rho)_y + \omega]\,\mathrm{d}A = 0, \tag{11b}$$

$$\iint W_3\{\nabla^2(\mu\omega) - Re[(\rho\Phi_x + \psi_y)\omega_x + (\rho\Phi_y - \psi_x)\omega_y + S_\rho]\}\,\mathrm{d}A = 0, \tag{11c}$$

where $W_1$, $W_2$ and $W_3$ are weight functions. The weight function $W_1$ is chosen as $N^{\Phi}$, $W_2$ is chosen as $N^{\psi}$, while $W_3$ is chosen as $N^{\omega}$, where $N^{\Phi}$, $N^{\psi}$ and $N^{\omega}$ are the finite element shape functions. Since the vorticity is the derivative of the velocity, it is preferable to use bilinear shape functions for $N^{\omega}$, i.e. the vorticity is to be represented at four corners, while $N^{\Phi}$ and $N^{\psi}$ are chosen as biquadratic, i.e. the potential and the stream function are to be represented at eight nodes. The geometry is described by eight nodes. Hence

$$\Phi=\sum_1^8 N_i^{\Phi}(\xi,\eta)\Phi_i, \qquad \psi=\sum_1^8 N_i^{\psi}(\xi,\eta)\psi_i, \qquad \omega=\sum_1^4 N_i^{\omega}(\xi,\eta)\omega_i, \tag{12a}$$

$$x=\sum_1^8 N_i^{\Phi}(\xi,\eta)x_i, \qquad y=\sum_1^8 N_i^{\Phi}(\xi,\eta)y_i, \tag{12b}$$

where $(\xi,\eta)$ are the non-dimensional co-ordinates of the parent (undistorted) finite element. The weak form is obtained after the integration by parts of equations (11a)–(11c). This yields

$$\iint \rho(W_{1_x}\Phi_x+W_{1_y}\Phi_y)\,\mathrm{d}A-\int W_1(\rho\Phi_n)\,\mathrm{d}s=0, \tag{13a}$$

$$\iint (W_{2_x}\psi_x/\rho+W_{2_y}\psi_y/\rho-W_2\omega)\,\mathrm{d}A-\int W_2(\psi_n/\rho)\,\mathrm{d}s=0, \tag{13b}$$

$$\iint \{W_{3_x}(\mu\omega)_x+W_{3_y}(\mu\omega)_y+W_3 Re[(\rho\Phi_x+\psi_y)\omega_x+(\rho\Phi_y-\psi_x)\omega_y+S_\rho]\}\,\mathrm{d}A-\int W_3(\mu\omega)_n\mathrm{d}s=0. \tag{13c}$$

*Newton linearization*

Using the Newton method, the linearized equations for the change in the variables $\Phi$, $\psi$ and $\omega$ are

$$\iint [W_{1_x}(\rho\Delta\Phi)_x+W_{1_y}(\rho\Delta\Phi)_y]\,\mathrm{d}A=-R_1, \tag{14a}$$

$$\iint [W_{2_x}(\Delta\psi)_x/\rho+W_{2_y}(\Delta\psi)_y/\rho-W_2\Delta\omega]\,\mathrm{d}A=-R_2, \tag{14b}$$

$$\iint \{W_{3_x}(\mu\Delta\omega)_x+W_{3_y}(\mu\Delta\omega)_y+W_3 Re[\psi_y(\Delta\omega)_x+\omega_x(\Delta\psi)_y-\psi_x(\Delta\omega)_y-\omega_y(\Delta\psi)_x+\rho\Phi_x\Delta\omega_x+\rho\Phi_y\Delta\omega_y]\}\,\mathrm{d}A=-R_3, \tag{14c}$$

where $R_1$, $R_2$ and $R_3$ are the residuals of equations (3), (4) and (5) respectively.

Substituting the shape functions, one obtains

$$\sum_{j=1}^{8} K_{1ij}\Delta\Phi_j=-R_{1i}, \tag{15a}$$

where

$$K_{1ij}=\iint(\rho W_{1i_x}N_{j_x}^{\Phi}+\rho W_{1i_y}N_{j_y}^{\Phi})\,\mathrm{d}A;$$

$$\sum_{j=1}^{8} K_{2ij}\Delta\psi_j+\sum_{j=1}^{4} K_{3ij}\Delta\omega_j=-R_{2i}, \tag{15b}$$

where

$$K_{2ij}=\iint (W_{2i_x}N^{\psi}_{j_x}/\rho + W_{2i_y}N^{\psi}_{j_y}/\rho)\,\mathrm{d}A,$$

$$K_{3ij}=\iint (W_{2i}N^{\omega}_{j})\,\mathrm{d}A;$$

and

$$\sum_{j=1}^{4} K_{4ij}\Delta\omega_j + \sum_{j=1}^{8} K_{5ij}\Delta\psi_j = -R_{3i}, \tag{15c}$$

where

$$K_{4ij}=\iint \{W_{3i_x}(\mu_x N^{\omega}_{j}+\mu N^{\omega}_{j_x}) + W_{3i_y}(\mu_y N^{\omega}_{j}+\mu N^{\omega}_{j_y}) + Re\,W_{3i}[(\rho\Phi_x+\psi_y)N^{\omega}_{j_x}+(\rho\Phi_y-\psi_x)N^{\omega}_{j_y}]\}\,\mathrm{d}A,$$

$$K_{5ij}=\iint Re[W_{3i}(\omega_x N^{\psi}_{j_y}-\omega_y N^{\psi}_{j_x})]\,\mathrm{d}A.$$

The terms of the influence matrix must be integrated numerically. A typical term of the influence matrix is evaluated as

$$K_{ij}=\int_{-1}^{1}\int_{-1}^{1} F_{ij}[x(\xi,\eta), y(\xi,\eta)]\,|J|\,\mathrm{d}\xi\,\mathrm{d}\eta, \tag{16}$$

where both $[J]$ and $[J]^{-1}$ are explicitly calculated at the Gaussian points of each element and the numerical integration is carried out using $3\times 3$ Gaussian integration points.

## BOUNDARY CONDITIONS

At the inlet and exit the Dirichlet boundary conditions for both the stream function and vorticity (6b, 6c, 7a) are accounted for in the standard way, while the Neumann boundary conditions (6a, 7b, 7c) make the contour integrals vanish.

For the remaining boundary conditions a difficulty exists since there are three conditions on $\psi$ and $\omega$ at the edge of the viscous region and no explicit condition on $\omega$ at the solid surface. If the $(\psi$–$\omega)$-equations are solved simultaneously, it is not important how the boundary conditions are introduced in the matrix. Taking advantage of this, the rows of unknown vorticities on the walls are replaced by condition (10a), while conditions (10b) and (10c) are implemented in a standard way. One should note that this completely avoids the need for wall vorticity formulae. The no-slip condition (9b) is implemented by replacing $\psi_n/\rho$ in (13b) by its iteratively calculated value; hence the contour integral becomes

$$+\int W_2\Phi_s\,\mathrm{d}s. \tag{17}$$

The contour integral of (13a) is carried out analytically at the inlet and calculated at the walls from the stream function field at every iteration as

$$-\int W_1\psi_s\,\mathrm{d}s, \tag{18}$$

which bears similarity to a transpiration boundary condition in viscous–inviscid interaction methods.

A note should be added here about boundary conditions for the velocity potential for choked flows. Since the velocity potential formulation in the core does not allow for an entropy rise, the shock position is arbitrary since the only pressure that can be achieved at the exit is the isentropic one. To allow for non-isentropic flow, it is shown in Reference 9 that a Dirichlet boundary condition on $\Phi$ must be imposed at the exit and its value must be iterated upon until the imposed back-pressure is satisfied by the numerical solution.

## SOLUTION METHODOLOGY

### *Updating the pressure*

The pressure can be obtained from the following relation:

$$p=[1-\tfrac{1}{2}(\gamma-1)M_\infty^2(\Phi_x^2+\Phi_y^2-1)]^{\gamma/(\gamma-1)}/\gamma M_\infty^2. \tag{19}$$

This dispenses with the solution of an equation for the pressure at the expense of neglecting the viscous contribution to the pressure variation across the boundary layer. Should a more exact solution be needed, a method discussed in Reference 10 for determining the pressure from a Poisson equation could be used.

### *Updating the density*

Under the assumption of constant total enthalpy,

$$\gamma p/(\gamma-1)\rho+\tfrac{1}{2}(u^2+v^2)=H_\infty. \tag{20}$$

The density is obtained from this equation once the pressure has been determined. Equation (20), while exact for inviscid flows, is a reasonable approximation for the viscous energy equation in the absence of heat exchange. This should not be construed as a limitation of the present method, since the complete energy equation can be solved without difficulty if needed. One should note that the density assumes its profile in the boundary layer and reduces smoothly to the isentropic relationship in the potential core.

For supersonic points the density $\rho$ in the potential equation is replaced by a shifted density $\bar{\rho}$ to add the artificial viscosity necessary for shock wave simulation:

$$\bar{\rho}_e=\rho_e-\mu(\rho_e-\rho_{e-1}), \qquad \mu=\max(0, 1-(1/M_e^2), 1-(1/M_{e-1}^2)). \tag{21}$$

Note that the potential equation is the only equation in which artificial viscosity is introduced.

### *Turbulence modelling*

To include the effects of turbulence, the Baldwin–Lomax model is used.[10] This model does not require the specification of a boundary layer thickness and hence presents particular advantages for internal flows. Details of the model will not be given here; they are outlined in Reference 10. However, it should be noted that the distance from the wall, which appears often as a parameter of turbulence models, is measured in the present work by moving away from the wall along equipotential lines obtained from the initial solution of (14a).

### *Solution strategy*

The procedure consists of solving the ($\psi$–$\omega$)-system simultaneously, while the $\Phi$-solution is lagged. The problem is started at $Re=0$ and marched through $Re=10^n$ from $n=1$ to the

target *Re*. The turbulent viscosity is updated at every iteration. The pressure and density are obtained from (19) and (20). The $(\psi-\omega)$-calculations are limited only to a relatively thin layer near the walls with a fine mesh, dictated by resolution and accuracy requirements. The velocity potential, defined throughout the field, can be solved on a coarse grid and interpolated if required onto the finer $(\psi-\omega)$-grid.

## RESULTS

Results of the method are presented for compressible and transonic internal flows. The first example is comparison between the present approach and the $(\Psi-\omega)$ full Navier–Stokes method of Reference 11 for subsonic viscous calculations. Next are calculations in choked nozzles with a comparison against the result of the viscous–inviscid interaction method of Le Balleur.[5]

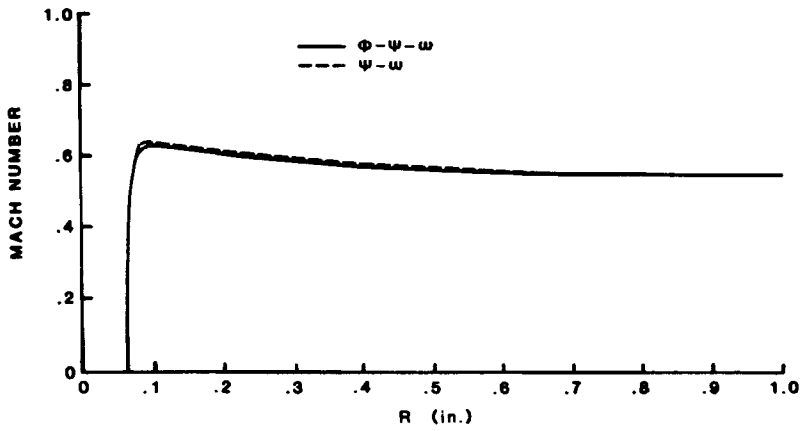


Figure 2. Comparison of Mach number profiles at maximum bump height: proposed approach $(\Phi-\psi-\omega)$ and full Navier–Stokes $(\Psi-\omega)$

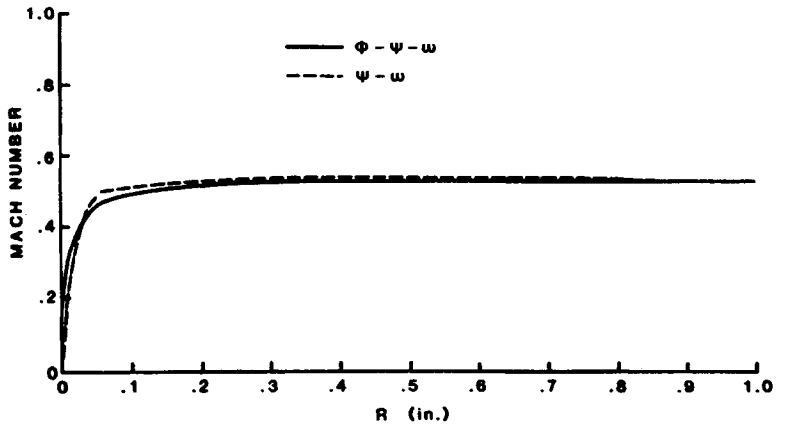


Figure 3. Comparison of Mach number profiles at trailing edge of bump: proposed approach $(\Phi-\psi-\omega)$ and full Navier–Stokes $(\Psi-\omega)$

Symmetric nozzles are chosen for the test cases, with the inlet velocity profile being a uniform flow with a Coles profile near each wall. Figures 2 and 3 compare the ($\Phi$–$\psi$–$\omega$)-results with those obtained using the full Navier–Stokes stream function–vorticity method of Reference 11 for the flow over a bump and indicate good agreement between the two methods. This lends credence to the present pressure approximation which avoids the solution of a Poisson equation for pressure. For subsonic flow, convergence to a residual of $10^{-6}$ is achieved in 15 iterations.

An example of the calculation of a choked flow in the same symmetric nozzle is shown in Figure 4. The inlet *Re* is 100 000 and the figure shows the Mach number contours at convergence indicating choking of the flow. The grid used is $30 \times 27$ elements. Convergence to a residual of $10^{-6}$ is achieved in 100 iterations. The velocity profiles are shown in Figure 5. The corresponding inviscid solution is shown in Figure 6.

A comparison with the viscous–inviscid procedure of Le Balleur[5] in the case of the choked duct is shown in Figure 7. The present approach displays some shock smearing because of the cruder grid that had to be used, $67 \times 27$ for the entire flow, while the grid used by Le Balleur has 100 grid

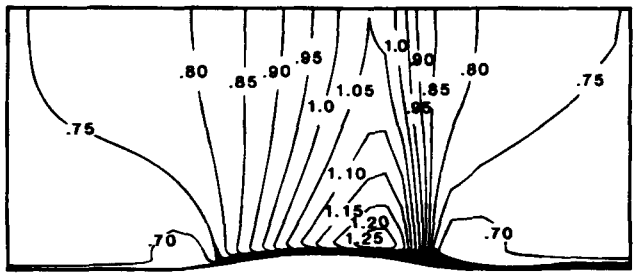


Figure 4. Choked viscous channel flow: Mach number contours for present viscous–inviscid approach ($\Phi$–$\psi$–$\omega$)

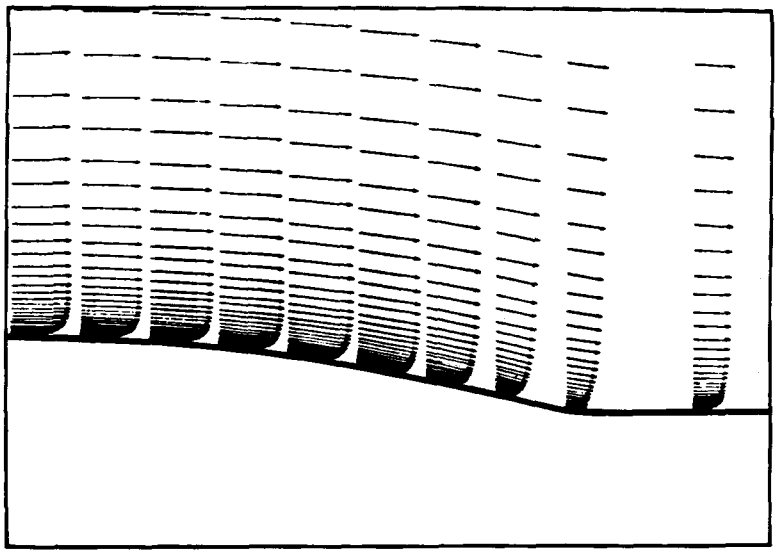

Figure 5. Choked viscous channel flow: Velocity profiles for present viscous–inviscid approach ($\Phi$–$\psi$–$\omega$)

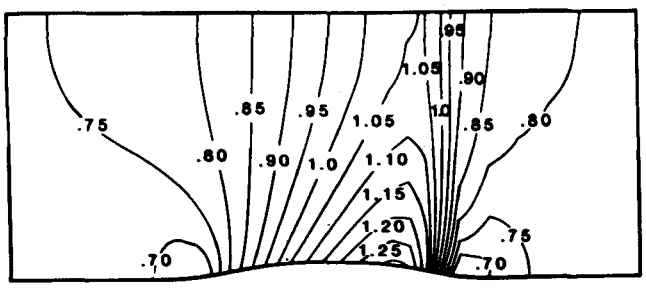


Figure 6. Choked inviscid channel flow: Mach number contours by potential solution ($\Phi$)

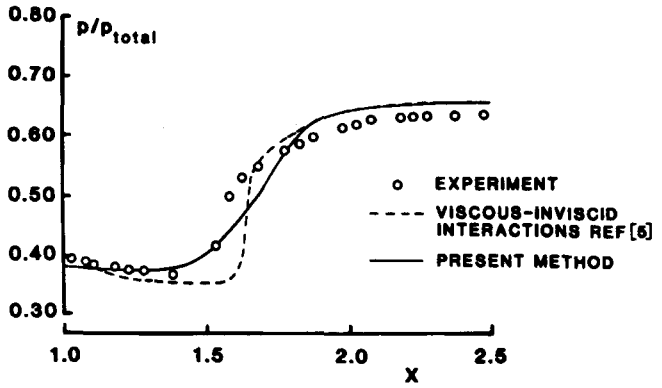


Figure 7. Comparison of wall pressure distribution for choked channel flow by viscous–inviscid interaction procedures: present approach ($\Phi$–$\psi$–$\omega$) versus Le Balleur[5]

points in the flow direction and his computational domain is restricted to only the shock wave–boundary layer interaction region. However, despite the differences in mesh size, the methods show good agreement in pressure distribution along the wall.

## CONCLUSIONS

It is shown that the application of a finite element method to a system of second-order equations for the velocity potential, the stream function and the vorticity can lead to efficient viscous flow calculations, with results comparable to Navier–Stokes solutions of high-Reynolds-number transonic flows. Stable solutions can be obtained with no upwinding for subsonic flows and with only upwinding in the potential equation for transonic flows. Moreover, explicit wall vorticity formulae are completely dispensed with.

This approach can be considered as a generalization of viscous–inviscid interaction procedures, with no boundary layer co-ordinates needed and no boundary layer approximations used. Moreover, the matching between the outer inviscid flow and the inner viscous region is automatic. This fact is manifested in the density determination, which reduces to the isentropic relationship in the potential core while capturing the boundary layer behaviour in the viscous regions.

An additional feature of this approach is the explicit calculation of the pressure from the velocity potential. While not describing the pressure profile inside the viscous region exactly, such an approximation is more accurate than the usual assumption of uniform pressure across the boundary layer. Should a more exact evaluation of pressure be required, a Poisson equation with natural boundary conditions can be solved.

ACKNOWLEDGEMENT

This work was partially supported under Operating Grant OGPIN013 of the Natural Sciences and Engineering Research Council of Canada (NSERC). The support of Pratt & Whitney Canada is also gratefully acknowledged.

## APPENDIX: NOMENCLATURE

| | |
|---|---|
| $A$ | domain area |
| $H$ | enthalpy |
| $\mathbf{K}$ | influence matrix |
| L-2 | residual norm $=\Sigma R^2$ |
| $M$ | Mach number |
| $N$ | finite element shape function |
| $n$ | outward normal to boundary |
| $p$ | pressure |
| $q$ | speed |
| $R$ | residual of a differential equation |
| $Re$ | Reynolds number |
| $s$ | distance along boundary of domain |
| $u, v$ | Cartesian velocity components |
| $x, y$ | Cartesian co-ordinates |
| $W$ | weight function for weighted residual method |

*Greek symbols*

| | |
|---|---|
| $\Delta$ | change in a quantity |
| $\Phi$ | velocity potential |
| $\gamma$ | isentropic exponent |
| $\mu$ | viscosity |
| $\rho, \bar{\rho}$ | density and shifted density respectively |
| $\psi$ | perturbation streamfunction |
| $\omega$ | vorticity ($\omega = v_x - u_y$) |

*Subscripts*

| | |
|---|---|
| $i.\ e$ | nodal and element index respectively |
| $n, s$ | derivative normal to and along boundary respectively |
| $x, y$ | $x$- and $y$-derivative respectively |
| $\infty$ | free-stream value |

## REFERENCES

1. R. W. MacCormack, 'A numerical method for solving the equations of compressible viscous flows', *AIAA Paper 69-3543*, 1969.
2. R. M. Beam and R. F. Warming, 'An implicit factored scheme for the compressible Navier–Stokes equations', *AIAA J.*, **16**, 393–402 (1978).
3. R. E. Melnik, H. R. Mead and A. Jameson, 'A multi-grid method for the computation of viscous–inviscid interaction on airfoils, *AIAA Paper 83-0234*, 1983.
4. R. Houwink and A. E. P. Veldman, 'Steady and unsteady separated flow computations for transonic airfoils, *AIAA Paper 84-1618*, 1984.
5. J. C. Le Balleur, 'Numerical flow calculation and viscous–inviscid interaction techniques', in W. G. Habashi (ed.), *Computational Methods in Viscous Flows*, Pineridge Press, Swansea, 1985, pp. 419–450.
6. D. E. Edwards and J. E. Carter, 'A quasi-simultaneous finite difference approach for strongly interacting flow', *Proc. 3rd Symp. on Numerical and Physical Aspects of Aerodynamic Flows*, T. Cebeci (ed.), California State University, Long Beach, CA, 1985, pp. 63–73.
7. D. Lee and R. H. Pletcher, 'Simultaneous viscous/inviscid interaction calculation procedure for transonic turbulent flows', *AIAA J.*, **26**, 1354–1362 (1988).
8. L. B. Wigton and M. Holt, 'Viscous–inviscid interaction in transonic flow', *AIAA Paper 81-1003*, 1981.
9. W. G. Habashi, M. M. Hafez and P. L. Kotiuga, 'Computation of choked and supersonic turbomachinery flows by a modified potential method', *AIAA J.*, **23**, 214–220 (1985).
10. B. F. Baldwin and H. Lomax, 'Thin layer approximation and algebraic model for separated turbulent flows', *AIAA Paper 78-257*, (1978).
11. W. G. Habashi, M. F. Peeters, G. Guevremont and M. M. Hafez, 'Finite element solutions of the compressible Navier–Stokes equations', *AIAA J.*, **25**, 944–949 (1987).